Acta Geodyn. Geomater., Vol. 17, No. 1 (197), 5–18, 2020
DOI: 10.13168/AGG.2019.0041
journal homepage: https://www.irsm.cas.cz/acta

ORIGINAL PAPER

EVALUATION OF DEFORMATIONS IN THE URBAN AREA OF OLSZTYN USING SENTINEL-1 SAR INTERFEROMETRY

Beata WIECZOREK

University of Warmia and Mazury in Olsztyn, Faculty of Geodesy, Geospatial and Civil Engineering, Institute of Geoinformation and Cartography, Oczapowskiego 2, 10-719 Olsztyn, Poland

*Corresponding author's e-mail: beata.zero@uwm.edu.pl

ARTICLE INFO

Article history:
Received 20 September 2019
Accepted 19 November 2019
Available online 11 December 2019

Keywords:
Monitoring urban infrastructures
Radar interferometry
Deformation maps
Land subsidence

ABSTRACT

The paper presents an analysis of the possibilities of using a data set of Sentinel-1 (S-1) Interferometric Synthetic Aperture Radar (InSAR) for urban monitoring. The study was conducted in the Olsztyn area, where by using the PSI (Persistent Scatterer InSAR) method the amount of deformation was determined, calculated using a multi-time SAR data series. Displacement values were estimated by reducing error sources related to temporal and geometrical decorrelation and atmospheric phase delay.

Based on the defined assumptions, three calculation cases were prepared. This processing is based on the data from more than 648 Sentinel-1A/B images over ascending and descending orbits acquired between October 2014 and August 2018 to determine the value of the Line of Sight (LOS) ground deformation rates. Regular acquisition of SAR images from the Sentinel-1 satellite sensor in an interval of 2 days enabled the detection of more than 1000 PSI points per 1 km^2 in the 10 × 10 km^2 urban area. The mean LOS velocity of surface change was determined on the basis of four large data sets. Comparable values were obtained from ascending tracks 29, 102 and descending tracks 51, 124 where mean velocity ranges respectively: A29 from -4.3 to 3.4 mm/yr, A102 from -3.9 to 3.5 mm/yr and D51 from -3.9 to 3.1 mm/yr, D124 from -3.8 to 3.2 mm/yr. Then the results of geometries were combined in pairs to compute the actual vertical motion component.

In the presented work, an analysis of the terrain deformation was performed for selected characteristic objects located within the Olsztyn area. In the first case study, a detailed analysis of urban infrastructure facilities was carried out, including buildings and a section of the railway line. The other case study covers an area along the river bank. A large number of observations allowed to accurately determine the deformation model and to produce the history of deformations on the tested area, based on the analysis of time series of interferograms.

The paper presents solutions using InSAR data in urban monitoring and shows why this technology is a useful tool for studying measuring urban subsidence. The results are displayed in the form of a deformation map showing the magnitude of the measured movement.

INTRODUCTION

The ability to detect land displacements that have occurred locally, regionally, or even nationally, is very important in characterizing endangered areas. Therefore, the InSAR technique is useful for generating precise height digital elevation models (DEM) and monitoring long-range surface deformations (Ferretti et al., 1999). It uses interferometric comparison of phases of SAR images, determined in time intervals for the same object from slightly different positions (Zebker et al., 1992). Based on the phase differences of the corresponding radar signals information is obtained about relative values of the elevation of the terrain surface or its changes over time with millimeter accuracy (Monti-Guarnieri et al., 1993). InSAR limitations result mainly from the time and geometrical de-correlation and inhomogeneity of the atmosphere. The time de-correlation affects the gradual loss of coherence over time, which is linked to changes in electromagnetic properties or/and the position of the diffuser within the resolution cell. The geometric decorrelation limits the number of image pairs suitable for interferometric applications and prevents the full use of the available data set (Ferretti et al., 2001). Another limitation is related to the fact that InSAR measurements are prone to atmospheric errors. RADAR waves traverse the Earth's atmosphere twice and experience a delay due to atmospheric refraction. The two major layers of the atmosphere (troposphere and ionosphere) that are mainly responsible for this delay are the source of the phase component of the Atmospheric Phase Screen (APS) signal (Krishnakumar et al., 2018). In the case of a single interferogram or only a few interferograms for a given area, atmospheric effects are very difficult or even impossible to remove, hence the obtained

Cite this article as: Wieczorek B: Evaluation of deformations in the urban area of Olsztyn using Sentinel-1 SAR interferometry. Acta Geodyn. Geomater., 17, No. 1 (197), 5–18, 2020. DOI: 10.13168/AGG.2019.0041

measurement accuracies are often much lower than expected (Hanssen, 2001). To reduce the basic errors, methods based on SAR time series analysis are used, which allow reproducing the course of deformation of a given area. This approach ensures data redundancy and enables decomposition of the interferometric phase into components (Bamler et al., 1999) and determination of deformation increments with very high accuracy (even 1 mm/yr) (Ferretti et al., 2007).

Many Multi-Temporal InSAR (MTI) algorithms have been developed that differ in the processing strategy and the selection of coherent pixels in time. In scientific research, to determine the amount of deformation based on multi-time analysis of the SAR data series, methods based on two basic algorithms are used: Permanent Scatterer Interferometry (PSI) (Ferretti et al., 2001) and SBAS (Small Baseline Subset) (Berardino et al., 2002). A review of several algorithms time series analysis of InSAR data can be found in (Osmanoğlu et al., 2016) including the following algorithms: Coherent Pixels Technique (CPT), Delft Persistent Scatterer Interferometry (DePSI), Interferometric Point Target Analysis (IPTA), Permanent Scatterer InSAR (PSInSARTM), Persistent Scatterer Pairs (PSP), Quasi Persistent Scatterers (QPS), Small Baseline Subset (SBAS), Stable Points Network (SPN), SqueeSARTM, Stanford Method for Persistent Scatterers (StaMPS) and Corner Reflectors InSAR (CRinSAR).

Currently, the InSAR technique is used to monitor movements on a local scale caused by human activity (Ferretti, 2014). Infrastructure monitoring is, in general, performed using Permanent Scatterer lnterferometry (Bischoff et al., 2019). This method involves identification of image pixels, coherent over long time intervals (Ferretti et al., 2011).

A Permanent Scatterer (PS) is defined as a radar target, within a resolution cell, that displays stable amplitude properties and coherent signal phase, throughout all of the images within a data stack (Tre Altamira, 2010). The high coherence is accompanied by a very high backscattering of the radar signal values, these are bright pixels in the images. Objects that make good PS are varied and can be natural or man-made. Permanent Scatterer correspond to such objects as buildings, fragments of various types of structures (bridges, fences, etc.), high telegraph poles or lanterns, and specially designed corner reflectors. In areas without infrastructure, among the natural forms PS points can be e.g. rock outcrops, hard un-vegetated earth surfaces, and boulders. The PS pixels are characterized by a very stable phase of the radar signal, almost insensitive to changes in imaging geometry and atmospheric conditions (Perski and Wojciechowski, 2017).

Until recently, the main factor limiting the advanced analysis of InSAR time series was the inaccessibility of a homogeneous SAR base on a national or continental scale (Haghighi and Motagh, 2017). The launch of Sentinel-1A in 2014, followed by Sentinel-1B in 2016, as part of the Copernicus mission (an initiative of the European Commission (EC) and the European Space Agency (ESA)) influenced the availability of SAR data. The mission provides an independent operational capability for continuous radar mapping of the Earth. The Sentinel-1 mission includes C-band imaging operating in four exclusive imaging modes with different resolution (down to 5 m) and coverage (up to 400 km). It provides dual polarisation capability, very short revisit times (6 days) and rapid product delivery. For each observation, precise measurements of spacecraft position and attitude are available (ESA Standard Document, 2013). Synthetic Aperture Radar (SAR) is a microwave imaging system, it has day and night operational capabilities because it is an active system. System configuration allows accurate measurements of the radiation travel path because it is coherent (Goldstein, 1995). The mission provides enhanced revisit frequency, coverage, timeliness and reliability for operational services and applications requiring long time series. The Sentinel-1 the first sensor was specifically designed for surface deformation monitoring over large areas (Ferretti et al., 2015). Every day, over 10 TB of SAR data products are delivered and will be updated until 2035 (Annex to the Commission, 2018).

The main objective of the research was to check the capability of the European space mission in obtaining information on relative altitude data in the Olsztyn area. In this work, the data set Sentinel-1A/B images over ascending and descending orbits, from the period from October 2014 to August 2018, were applied. To determine the value of the Line of Sight ground deformation rates, Stanford Method for Persistent Scatterers (StaMPS) (Hooper et al., 2004; Hooper et al., 2007) based on the PS and SBAS algorithm was applied. Estimation of the atmosphere-related errors was conducted by means of the Toolbox for Reducing Atmospheric InSAR Noise (TRAIN) (Bekaert et al., 2015). The study examines several urban infrastructure facilities for which displacement analysis was performed using S-1 InSAR time series.

MEASUREMENT OF DEFORMATION RATES

The study area covers the city of Olsztyn located in North-Eastern Poland, an area of approximately 10×10 km^2. The geology of the region is characterized by mainly tills, and glacial and outwash sands and gravels. There are numerous surface waters in the studied area, which take about 10 % of the surface, moreover, almost the entire area is within the range of the quaternary Main Groundwater Reservoir (Nowicki, 2007). Figure 1 shows the location of the studied area as well as the geological and hydrological characteristics that affect the stability of the ground.

Research on the speed of terrain deformation regards the period from October 2014 to August 2018. The data set adopted for analysis consists of 647 images covering the Olsztyn area, with a time interval of about 2 days, obtained from a SAR-C sensor (~ 5.5465763 cm) mounted on Sentinel-1A/B

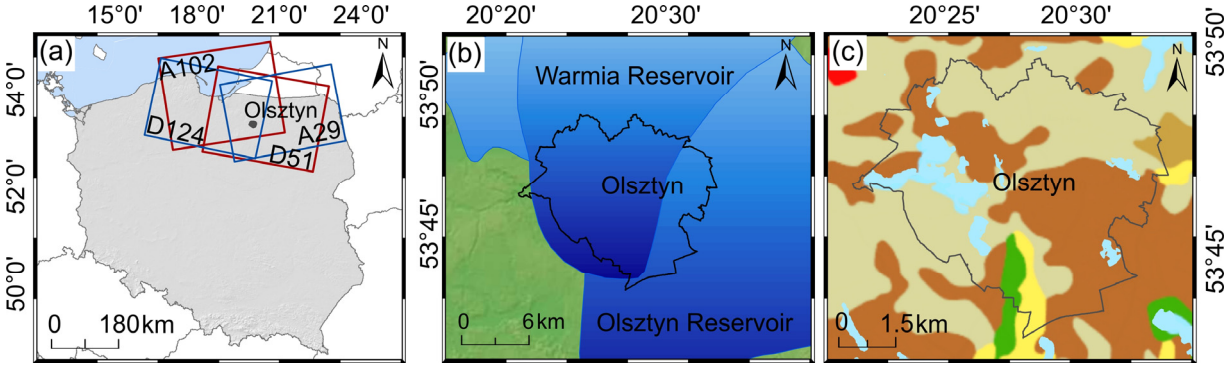

Fig. 1 Location of the research area shown in the map of Poland and the range of the Sentinel-1 ascending (A29 and A102) and descending (D51 and D124) orbits, ascending and descending tracks were selected and combined in pairs for which the study area is mapped by means of comparable incidence angles (A29 and D124) and (A102 and D51). (b) The range of Warmia and Olsztyn, two reservoirs located within the analyzed area. (c) Geological characteristics of the region: the greater part of the area is covered by tills, weathered tills and glacial sands and gravels (brown color), the area from NW to SE is occupied by outwash sand and gravel (beige color). In the south of the area there is a small field where the main soil composition is: kame sands and silts (yellow color), fluvial sands, gravels, muds, peats and organic silts (green color).

Table 1 Sentinel-1 SAR dataset used to study displacements in Olsztyn.

Connected paths	Track	Orbit Pass (Ascending/ Descending)	Acquisition date	Heading (α°)	Incidence angle (θ°)	Number of interferograms
Pair 1	29	A	19.10.2014 – 29.08.2018	349	34	165
	124	D	14.10.2014 – 30.08.2018	192	32	160
Pair 2	102	A	12.10.2014 – 28.08.2018	350	42	166
	51	D	21.10.2014 – 31.08.2018	190	40	153

satellites. S-1 products are not synchronized spatially, which means that their start and end times differ within each orbit. Besides, often more than one scene is required to fully cover the Olsztyn area.

Two frames of ascending (A29, A51) and two frames of descending (D102, D124) Sentinel-1 data were selected for the study to investigate the dynamics of terrain dislocations within the last 4 years. Basic information on the dataset for the analyzed paths is provided in Table 1.

Surface change was measured on the basis of the study of radar interferometry satellite images, which include the Olsztyn area. Approximately 160 interferograms were calculated for each path of Sentinel SAR images, which provided usable data to analyze surface subsidence. Figure 2 shows that the velocity values are relative to the mean velocity of the whole image for all paths from 10.2014 till 08.2018, showing subsidence reaching from about -4 to 3.3 mm/yr over an area of ~ 580 km^2.

Vegetation areas include less coherent PS points; so, there are some regions without sufficient outputs in the extracted maps. Figure 2 shows one coherent area in which PS points with high density were determined. It is a built-up area of the city of Olsztyn, because Permanent Scatterers are usually physical objects such as buildings, communication and technical infrastructure. All measurements are made in the LOS of the satellite's radar beam and are relative to points that are stable. Once the data have been calculated, it is possible to develop the history of movement across the area of interest. This is achieved by sequential calculation of the relative displacement between an individual radar target and the reference point, throughout the entire period of the analysis (Tre Altamira, 2010). The deformation is relative in time and space, a time series of movement of a PS is shown in Figure 2 (e). The study area covers the area of Olsztyn, city in north-eastern part of Poland. A detailed analysis of selected urban infrastructure structures, including buildings, a section of the railway line and the area along the river bank that flows through the city center have been carried out.

SAR INTERFEROMETRY PROCESSING

Sentinel-1 can collect SAR images in different modes, the Interferometric Wide (IW) swath mode is the main acquisition mode over land. It acquires data with a 250 km swath with a spatial resolution of 5 m by 20 m in range and azimuth directions. For Olsztyn it was as follows: range spacing 2.33 m, azimuth spacing 13.88 m. IW mode captures three sub-swaths using the Terrain Observation with Progressive Scans SAR (TOPSAR) acquisition principle. A TOPS SAR image consists of three sub-swaths, and each sub-swath is formed from several slightly overlapping subsets called bursts. The individually focused complex burst images are included, in azimuth-time

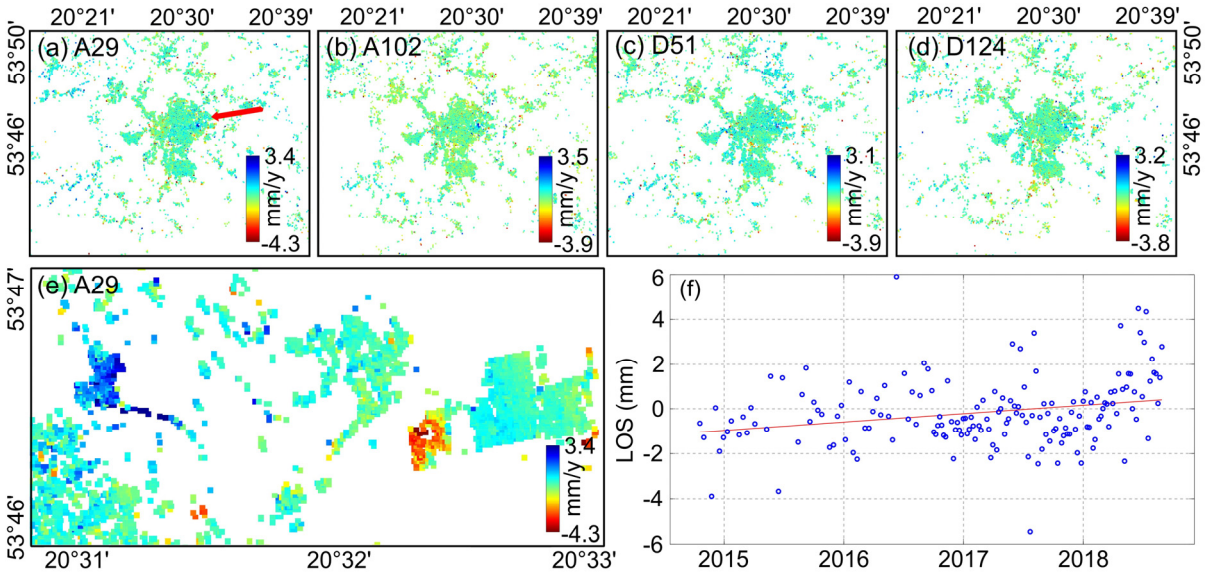

Fig. 2 (a)-(d) Sentinel SAR data from the C band obtained from four paths, showing surface change values measured between October 2014 and August 2018. Surface change for ascending tracks: (a) A29-4.3 to 3.4 mm/yr, (b) A102 -3.9 to 3.5 mm/yr and descending track: (c) D51 -3.9 to 3.1 mm/yr, (d) D124 -3.8 to 3.2 mm/yr. The average of all tracks gives -4 to 3.3 mm/yr subsidence rate. In Figure (a) in given area (red arrow) the value of the surface change is increasing and decreasing; see: movement of PS points within this area is plotted in Figures (e) and (f).

order, into a single sub-swath image with black-fill demarcation in between (ESA Standard Document, 2013).

In this research work interferometric processing of SAR data was divided into three stages:

Step 1: Pre-processing was performed in the SentiNel Application Platform (SNAP ESA http://step.esa.int). The pre-processing steps consist of forming a stack of co-registered single-master interferograms.

Step 2: PS Processing at this stage of work was performed by the implementation of the PSInSAR algorithm that is used in the Stanford Method for Persistent Scatterers (StaMPS). The basis of the PSInSAR method is to detect stable diffusers and then extract phase information for these points. This detection is based on multi-time amplitude analysis using the amplitude dispersion method (Ferretti et al., 2001), where the relationship between amplitude stability and interferometric phase stability (Hooper et al., 2004) as important property is applied. In this research work, significant parameters related to the characteristics of the input interferograms were estimated. The methodological and theoretical foundations of the procedure used in the StaMPS method were presented in (Hooper et al., 2004; Hooper et al., 2007a; Hooper et al., 2007b). The procedure consists of steps regarding:

- Estimation of the phase noise value for each candidate pixel in every interferogram. Pixels are selected on the basis of their noise characteristics. This step also estimates the percentage of random (non-PS) pixels in a scene from which the density per km² can be obtained. Pixels are weeded, dropping those that are due to signal contribution from neighbouring ground resolution elements and those deemed too noisy. Data for the selected pixels are stored in new workspaces. The wrapped phase of the selected pixels is corrected for spatially-uncorrelated look angle (DEM) error. At the end of this step the patches are merged.
- Phase unwrapping – unwraps interferograms.
- Estimation of spatially-correlated look angle error and master atmosphere and orbit error phase and noise. Estimation of spatially-correlated noise coming from atmospheric disturbances was performed in the toolbox TRAIN.

Step 3: Post-processing: calculations were carried out in Matlab, vertical movement components (up/ down) were determined from the observable values of the line of sight direction. The results were visualized in the ArcMap application and analysis and presentation of their interpretation was performed.

The sensor and platform characteristics include important parameters such as wavelength, bandwidth, Signal to Noise Ratio (SNR), orbit inclination, and repeat period (Hanssen, 2001). SAR sensors record both amplitude and phase of the backscattered radar echoes. The phase of a single SAR image is of no practical use. But if two SAR images from slightly different viewing angles are considered (interferometric pair), then their phase difference (interferometric fringes) can be usefully exploited to monitor terrain changes and to improve range resolution (Hanssen, 2001).

The SAR phase contains components from surface scattering and path delay. The scattering component is random between pixels, but the path delay is related to the radar geometry. The basis of InSAR is that by taking the phase difference of two SAR scenes, the difference in range can be obtained. Each SLC is acquired in a slightly different geometry, therefore, in order to ensure that the scattering phases cancel and that the correct pixels are interfered, the second SLC must be resampled to the coordinates of the first. This process is known as coregistration. If the images are not registered with sub-pixel accuracy then the interferometric signal will contain unwanted phase noise. Following coregistration, the phase difference is computed by a pixel-by-pixel conjugate multiplication between the first and second SLC (Wortham, 2014).

The interferogram contains the contributions from differential topographic height and differential ground deformation with respect to the reference pixel. The spatial and temporal disparities between the two SAR images will affect the interferometric phase and thus result in phase noise that can obscure desirable signals. The interferometric phase can be expressed by the following equation (1):

$$\Delta\varphi_{\text{int}} = \frac{4\pi}{\lambda}B_{\parallel} + \frac{4\pi}{\lambda}\frac{B_{\perp}\varepsilon}{R_0 \sin\theta} + \frac{4\pi}{\lambda}d_{los} + \\ + \Delta\varphi_{atm} + \Delta\varphi_{noise} + 2\pi k \tag{1}$$

where λ is the radar wavelength, R_0 is the slant range from the sensor to the target pixel, ε is the topographic height of the target pixel, θ is the incidence angle, $B_{\parallel}$ and $B_{\perp}$ are the parallel and perpendicular components of the orbit separation of the SAR image pair (baseline), respectively (Rosen et al., 1996). The first element represents the flat-Earth phase component, which is induced by the parallel baseline of the SAR image pair, and is a function of the pixel position regardless of topographic height. The second element represents the topographic phase component. The third element represents the deformation phase d_{los} (Hu et al., 2014). The component to be extracted, specifies the ground deformation along the LOS direction occurred in the time interval of the SAR image pair. In addition the signal noise ratio contains the atmospheric component delay $\Delta\varphi_{atm}$ and the phase noise $\Delta\varphi_{noise}$ is introduced by temporal change of the scatterers, different look angle, and volume scattering. The last element represents the phase of integer cycles and k is the integer ambiguity.

Deformation studies focus on the deformation phase d_{los} and make efforts to remove the topographic and atmospheric phases. Since the topographic phase component is proportional to elevation, one can determine the sensitivity of the interferometric phase to height ambiguity. So the height difference causing the interferometric phase change by 2π (one fringes). As the base distance increases, the interferometric phase sensitivity to topography increases. For each radar system, there is a critical interferometric base above which it is impossible to generate interferograms (Zebker et al., 1986). Therefore, smaller perpendicular baselines are preferred for deformation monitoring because they reduce the residual effect that might remain in interferograms by not completely removed topographic contributions, e.g. due to errors in the reference DEM (Haghighi and Motagh, 2017). The Sentinel-1 was designed to provide in small orbital InSAR baselines on the order of 150 m (Yagüe-Martínez et al., 2016) and as a result, the sensitivity of S-1 interferograms to inaccuracies of DEMs is low (Haghighi and Motagh, 2017). After removing the topographic phases using precise orbit information, existing DEMs, one obtains an interferogram. The resulting deformation usually has a magnitude greater than $\lambda/2$ which in the case of S-1 corresponds to ~2.8 cm in the direction of LOS. In order to measure a continuous deformation map, the phases between neighbouring pixels have to be integrated. Phase unwarping involves converting 2π cycles into quantities proportional to the actual heights by adding the appropriate total number of phase cycles to the phase value of each pixel. The InSAR observations given in slant-plane coordinates should be rectified or the measurements such as UTM or WGS-84 should be geolocated onto a uniform geodetic grid, to relate the slant-range measurements to ground coordinates.

The last component from the equation (1) to be estimated is the atmospheric component delay. The atmospheric phase contributions are spatially correlated within a single SAR scene, but tend to be uncorrelated on time scales of days to weeks. Conversely, surface motion is usually strongly correlated in time. C-band SAR images in midlatitudes are less susceptible to ionospheric effects, and hence the major atmospheric contribution in S-1 interferograms in mid-latitudes comes from the troposphere (Haghighi and Motagh, 2017). The routines available in the TRAIN (Bekaert et al., 2015) perform a horizontal and vertical spline interpolation for the pressure, temperature and relative humidity. The slant tropospheric delay is calculated by integrating the refractivity from the surface upwards, projected into the radar LOS (Vollrath et al., 2017), can be expressed as (2):

$$\varphi_{tropo} = -\frac{4\pi}{\lambda}\frac{10^{-6}}{\cos\theta}\int_{h1}^{h2}\left(N_{hydro} + N_{wet}\right)dh \tag{2}$$

where h_1 is the height of the target on SAR image, h_2 is the height of the effective tropospheric layer, and N_{hydro} and N_{wet} are refractivity corresponding to hydrostatic and wet delays.

The temporal and geometrical decorrelation of the signal limitations due to diverse phenomena, cause phase delays, which affects the readability of interferograms, and consequently surface change can be misinterpreted. Therefore, an analysis of the elements specified in formula (1), i.e. sources of phase

Table 2 Errors for ascending (A) and descending (D) tracks estimated by means of the StaMPS (Stanford Method for Persistent Scatterers) and TRAIN (the Toolbox for Reducing Atmospheric InSAR Noise).

	Component [mm/yr]							
	Mean LOS velocity [φ_{def}]		Orbital errors [φ_{orb}]		DEM errors [φ_{topo}]		Atmosphere [φ_{atm}]	
Track	min	max	min	max	min	max	min	max
29A	-4.399	3.377	-0.095	0.021	-0.036	-0.017	-0.008	-0.007
51D	-3.916	3.128	0.021	0.062	0.009	0.019	-0.033	0.013
102A	-4.040	3.510	-0.048	-0.012	-0.069	-0.042	-0.063	-0.039
124D	-3.823	3.239	-0.010	0.020	0.019	0.036	-0.001	-0.0004

Table 3 Calculated matrix for the first pair: A29-D124 and for the second: A102-D5.

	A29-D124		A102-D51	
Matrix A	0.829038	-0.595080	0.743145	-0.71207
	0.848048	0.529919	0.766044	0.642788

delay errors, was performed. They should be reliably estimated to identify PS pixels. The StaMPS framework is a collection of spatial and temporal filtering routines that allow to estimate each of these phase components by assuming a spectral structure. The individual quantities were calculated according to formula (1). As it was mentioned earlier the interferometric phase is determined by factors related to the topography, atmosphere, orbit and deformation. Their contribution is expressed by errors (estimated as annual average) and presented in Table 2.

As imposed by the acquisition geometry of SAR sensors on-board of satellite platforms, having a slanted view (tilted with respect to the vertical direction) referred to as line of sight (LOS), only part of the three-dimensional motion filed is captured (Foumelis, 2018). Therefore, the components of movement in the Vertical (Up) and E-W from the SAR LOS observables need to be determined. Computations require the use of at least 2 data sets with differing viewing geometries and look angles. A proper combination of data acquired along ascending and descending orbits allows to calculate these component of the displacement. In post-processing the ascending and descending PSI measurements (A29, D124) and (A102, D51) were paired them to calculate the vertical component for each individual PS point using equation (3) (Samiei-Esfahany et al., 2009; Budillon et al., 2018):

$$\begin{bmatrix} d_{los}^{asc} \\ d_{los}^{desc} \end{bmatrix} = A \cdot \begin{bmatrix} d_{up} \\ d_{h_{ald}} \end{bmatrix}; \rightarrow A = \begin{bmatrix} \cos\theta^{asc} & \frac{\sin\theta^{asc}}{\cos\Delta\alpha} \\ \cos\theta^{desc} & \sin\theta^{desc} \end{bmatrix}; \quad (3)$$

where d_{los} deformation along LOS, d_{up}vertical deformation, d_{hald} projection of horizontal deformation in descending azimuth look direction, θ incident angle, $\Delta\alpha$ satellite heading difference between ascending and descending mode. The values for individual angles are presented in Table 3.

The further processing workflow followed nearest neighbour vector (NNV) approach. The analysis concerned the identification of each point in one geometry and its nearest neighbour in the other geometry. The calculations included only one nearest point from two geometries, not the average of several nearest points, providing a simpler procedure and avoiding spatial smoothing of initial PSI measurements.

RESULT

The obtained average PSI LOS deformation rates for both ascending and descending tracks are presented in Figure 3. To verify their accuracy, a standard deviation of the mean LOS deformation velocities was determined. It was 0.67 mm/yr, 0.64 mm/yr for A29 and A102, respectively, and 0.61 mm/yr, 0.63 mm/yr for D51 and D124.

Then the results of geometries were combined in pairs to compute the actual vertical motion component. The average velocity map of the vertical deformation is presented in Figure 4. The combination of ascending and descending PS points was performed in the vector domain avoiding any rasterization option. The data coverage areas from both SAR geometries are different. Moreover, averaging values from multiple PS points available in each grid cell also smoothest the displacement field. Therefore, vector data was combined by using the nearest neighbour location and all operations were carried out using the transfer of attributes and calculations between the object's geodatabases.

In SAR data processing, the same parameters should be assumed for all developed paths. The selection criteria relate to the range of the development area and the assumed distance between points (nearest neighbour) of 20 m. Initially, PS stacks consisted of 119 146 and 130 453 points for the A29-pair D124, and with 147 107 and 158 77 points for the

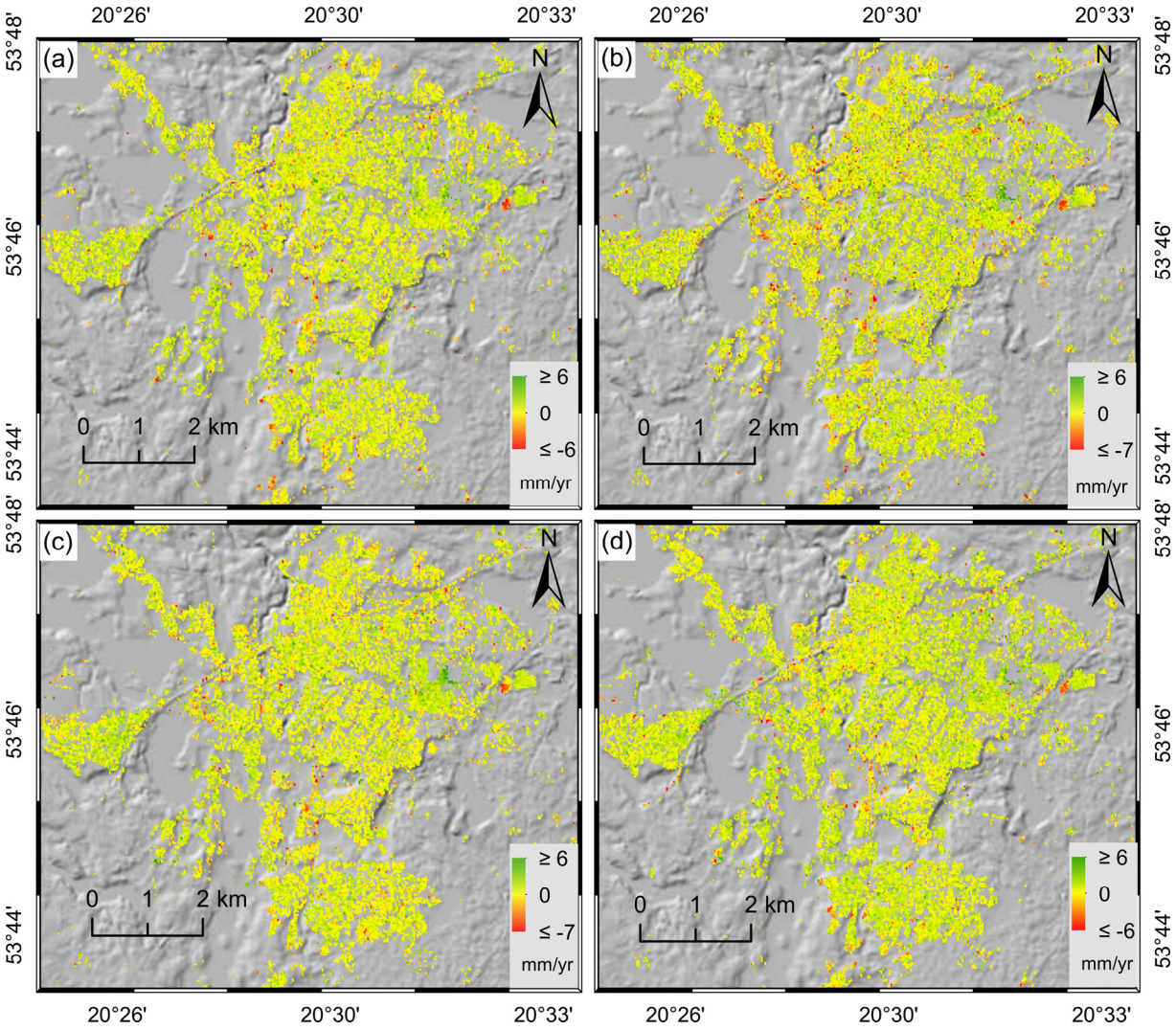

Fig. 3 (a)-(d) The visual display of results of a PS InSAR analysis for the building area in Olsztyn for A29 (a), D124 (b) and A102 (c), D51 (d), respectively. The colored dots represent the location of a PS, the color reflects the displacement rate measured at that point. Background image is from Geoportal WMTS ISOK Shading.

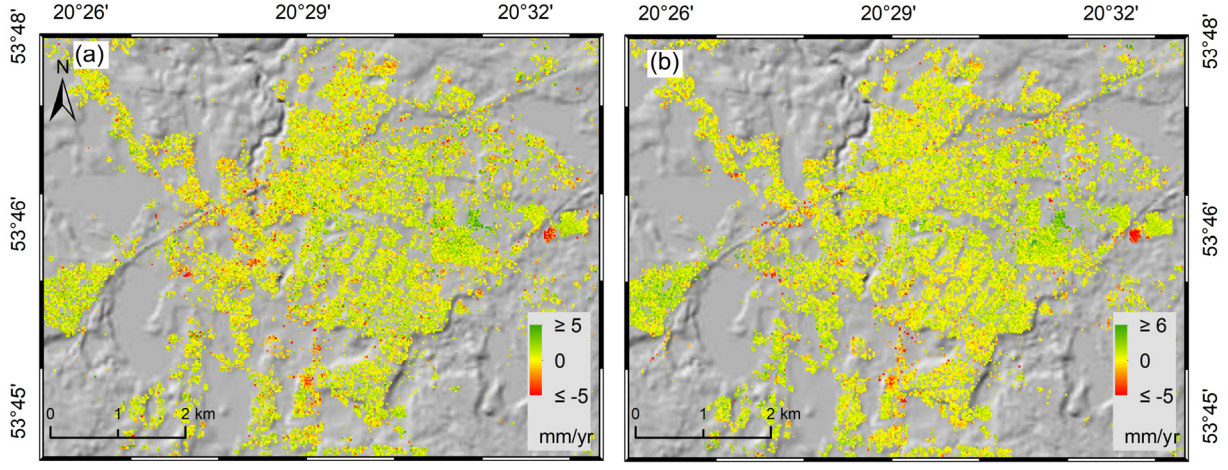

Fig. 4 Decomposition of LOS displacement to Vertical motion component, positive values correspond to uplift, (a) combined vector data-sets A29 and D124, (b) combined vector data-sets A102 and D51.

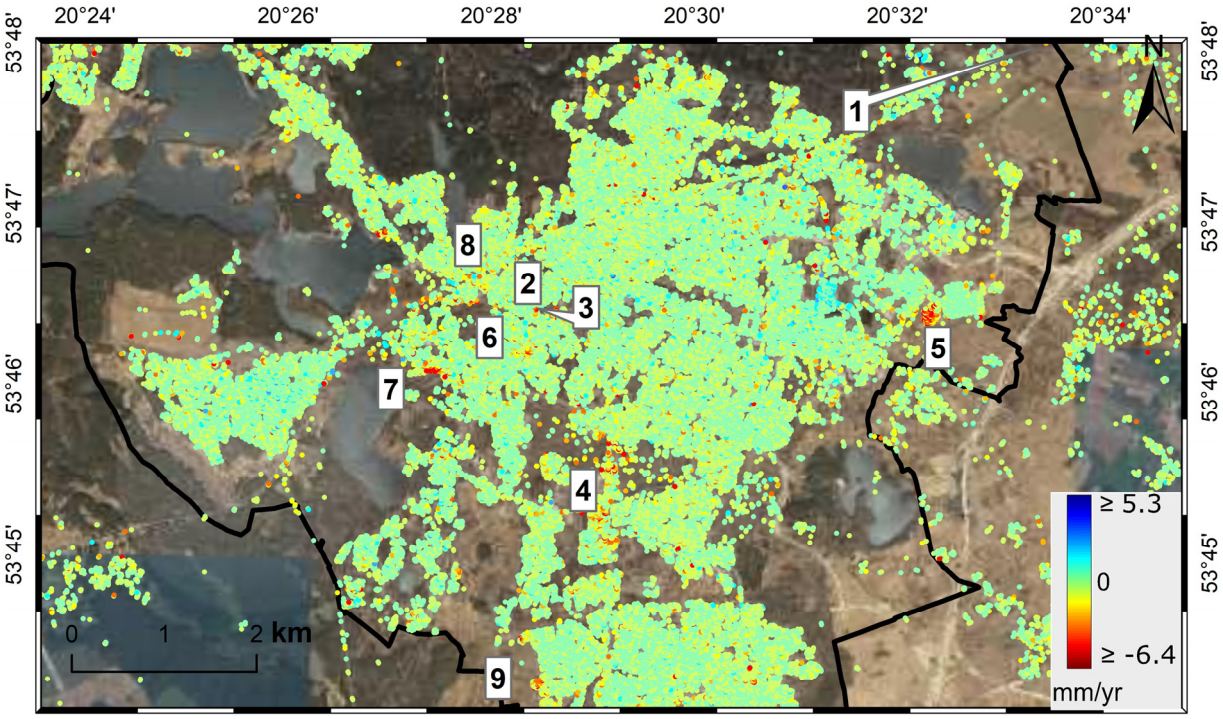

Fig. 5 Total displacement in the LOS, in millimeters, of 555 478 Permanent Scatterers based on 648 Sentinel-1 scenes gathered from 12 October 2014 to 31 August 2018. The displacement patterns show that, there is little ground movement across in Olsztyn (light green colours indicate 0 mm), but the different areas with higher subsidence can be clearly identified. The following areas were selected for the study: 1. fragment of the railway line (Figure 6); 2. area along the Łyna River (Figures 7 and 8); 3. a building in the city center (Figure 9). Background image is from Geoportal WMS Orthophotomap.

A102-D51 pair, respectively. In order to obtain the required consistent output PS data sets, a solution has been adopted that is a compromise between density of PS targets and requirements resulted from infrastructure monitoring. The number of points decreases significantly when data sets are combined. After the decomposition to actual motion component (Vertical) the total number of points was: 99 608 for A29, 94 411 for D124, 127 810 for A102, 123 821 for D51.

Calculations of the data obtained from the Sentinel-1 A/B satellites allowed to present the urban deformation with special attention to different areas subsidence. The results of an InSAR analysis were visualized by the geographic information systems tools, information about the extent of deformation were loaded into the vector layers of the Olsztyn area. Several examples are presented for which the observed deformation was calculated: Case study 1: fragment of a railway line; Case study 2: buffer area 200 m from the Łyna river bank within the Olsztyn area (the middle section of the river in the city center was selected for analysis); Case study 3: building located on the right bank of the Łyna River, on the south from the road crossing.

The locations of ascending and descending PS targets presented in Figure 5 were obtained by calculation of displacement in the Line of Sight from four tracks. A larger number of PS points allows for proper characteristics of deformation phenomena. Eventually, the LOS deformations from both, the ascending and descending tracks are presented in Figure 5. There is a noticeable line in the Olsztyn area, running from north to south (on the west side of the city) in which the movement up is visible (Fig, 5). This line coincides with the soil properties change line, where boulder clay, weathered, glacial sands and gravels change into sands and river-type gravels.

In addition, several important significant dip areas have been identified by the markings in Figure 5, such as: 4. a complex of commercial facilities at Sikorskiego Street; 5. area of the production plant located in the eastern part of the city; 6. a building at the corner of Warszawska and Śliwa streets; 7. residential building at Armia Krajowa Avenue; 8. zone from Lake Długie to The Railway Bridge over the Łyna (The railway bridges Łyna); 9. residential buildings in the western part of the Osiedle Generałów. It can be seen that that various deformation patterns exist, attributed to the different subsidence mechanisms acting in the area of Olsztyn. In this paper, the causes of slight deformation in the area of interest were not investigated. The following figures (Figure 6-9) show surface displacement over a range of sites.

Case study 1: The railway infrastructure in Olsztyn consists of four lines: Poznań East-Skandawa running from west to east, Olsztyn Główny-Bogaczewo towards north, Olsztyn Główny-Ełk towards S-E and the Olsztyn Główny-Działdowo line

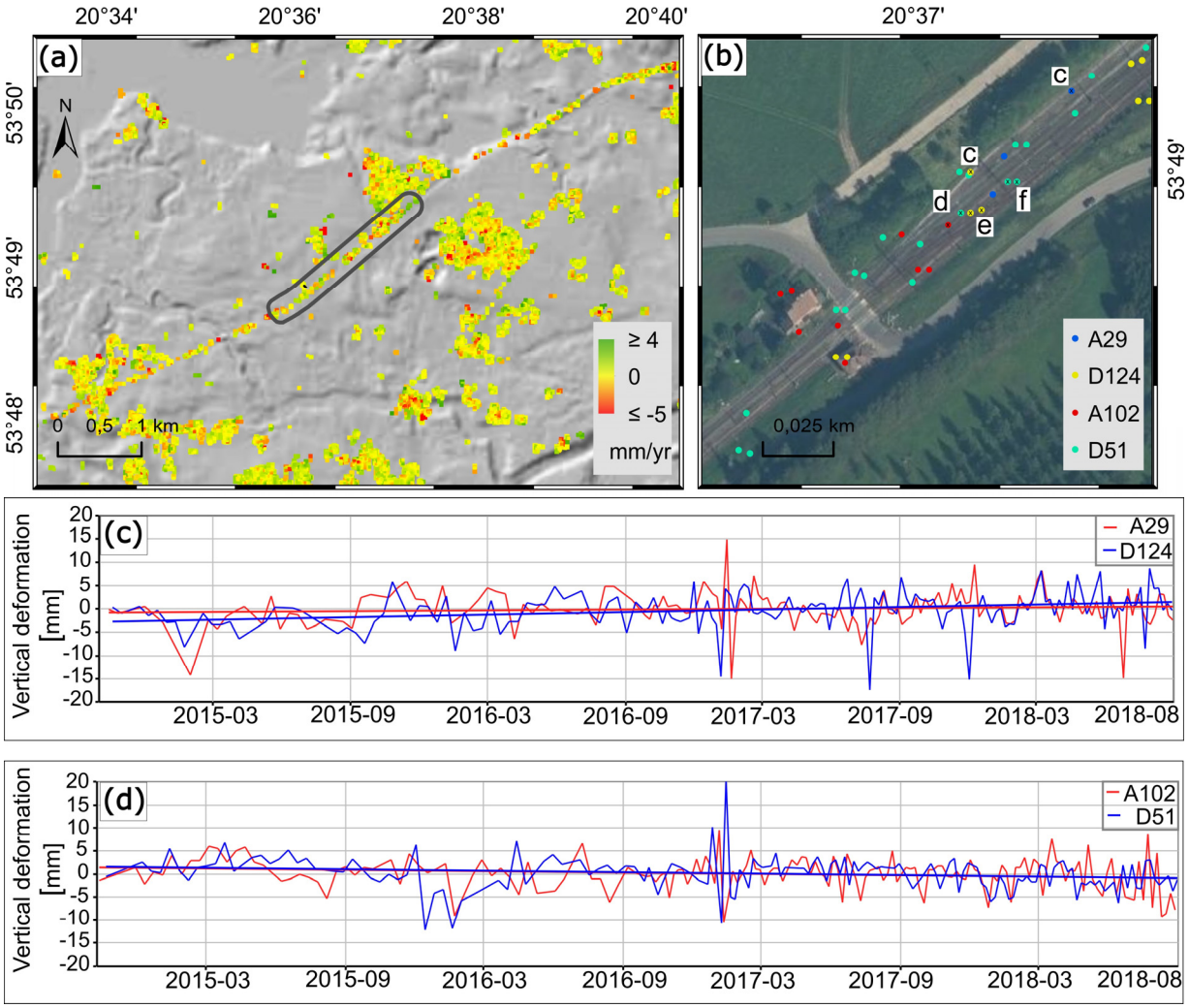

Fig. 6 Correlation coefficients between the track gauge 1 and track gauge 2, it regards to points presented in Figure 6 (b). Blue circles represent the data dispersion and area marked by the red lines indicates 95 % confidence interval of the regression line.

towards south. An analysis of a fragment of the Poznań-Skanda line, located in the northern part of Olsztyn, was performed. To visualize the changes that take place on the railway line section, time series of several selected PS points in the area of interest were plotted. Displacement rate measured at points with ascending and descending track were determined, located nearby, on one rail.

Time series of PS points for pairs A29-D124 and A102-D5 were drawn (Figure 6 (c) and (d)). In the case of the A29-D124 pair, it has been observed that the values of terrain deformation from January 2018 are similar and the graphs coincide. The trend for both paths is increasing. The mean trends of change were obtained for this track fragment, ranged from +0.31 ± 0.33 mm/yr for A29, from +1.15 ± 0.31 mm/yr for D124. For the A102-D51 pair on the second track, here the convergence of measurements has been visible since February 2017, while the trend is decreasing and coincides for both paths, for A102 it was from -0.62 ± 0.28 mm/yr, for D51 from -0.80 ± 0.33 mm/yr.

In Figure 6 (c) and (d) both large changes in surface are visible in January 2017. As can be seen from the graph in Figure 6 (c) in PS point from A29 there are largest differences of deformation from -14.86 to 15.09 mm. The cause of it was not analyzed in this work.

Another study concerned the determination of compliance of measurements taken from one path for two rails of one track. An analysis of the measured PS points for descending track 124 and 51 was performed. For D124 a correlation coefficient of 0.82 was achieved at a distance between points of 4.10 m, while for D51 the correlation coefficient was 0.80 at a distance between points of 3.92 m. Figure 7 shows the correlations between the measurement of the PS point on the first and second rail of a railway track (2014-2018).

Case study 2: The vertical deformation for the buffer zone of 200 m from the river was separated from the area (Fig. 8). The vector layer of the river shape was obtained from the base of the Polish Water Farm Wody Polskie. The Łyna River in the area of

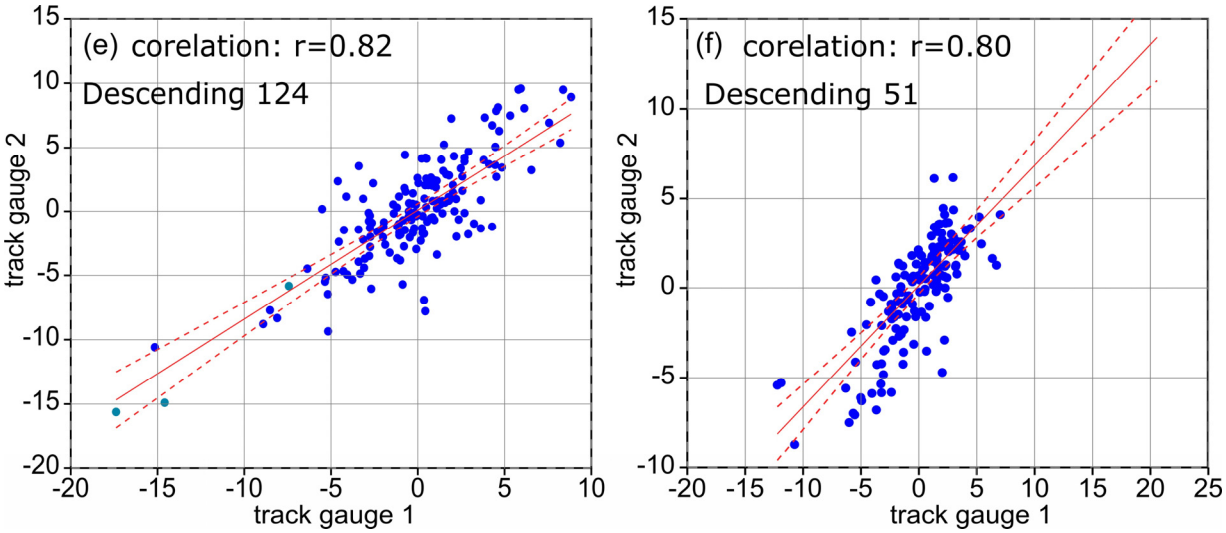

Fig. 7 Correlation coefficients between the track gauge 1 and track gauge 2, it regards to points presented in Figure 6 (b). Blue circles represent the data dispersion and area marked by the red lines indicates 95 % confidence interval of the regression line.

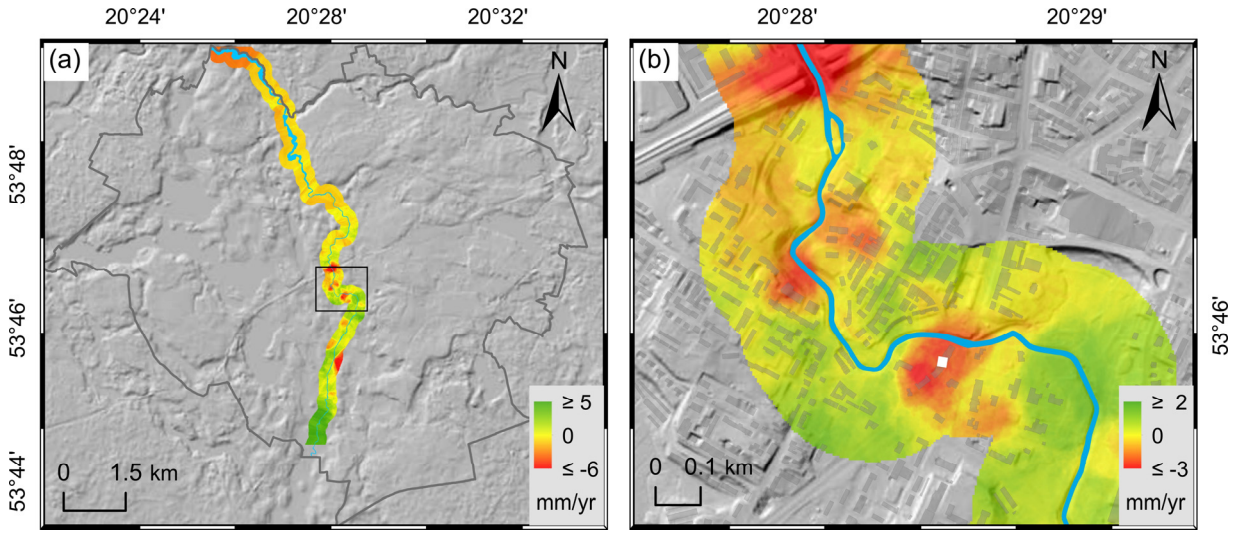

Fig. 8 Area along the Łyna River (a) buffer zone in the distance of 200 m from the river (yellow colors indicate 0 mm), black square shows the location of area in the city center, (b) area where significant movement, both up and down was determined. White square in (b) defines the building, which is shown in Figure 9. Background image is from Geoportal WMTS ISOK Shading and vector layer with buildings from MODGiK Olsztyn.

interest has a width of 5 to 30 m, flows through the city center. There are low and medium buildings are located on the right and left bank of the river.

To obtain a continuous displacement surface in the river area, a GRID mesh was created for which vertical motion component interpolation was performed. During interpolation, accuracy decreases, but values are obtained, especially in regions where PS points were missing. Interpolation was performed on PS target together for two pairs (A29-D124, A102-D51). Significant deformation is revealed in the city center from -3 to 2 mm/yr and in the north of the area to -6 mm/yr. In the southern part there is movement up to 5 mm/yr. In the remaining buffer zone there is stable or irrelevant deformation.

Case study 3: In the example, an analysis was made of the building, which is located in the city center by the road and by the river bank (Fig. 9). The building is approximately 8 m from the river bank. Settlement is quite common in built-up areas along the river floodplains. Most of the buildings by the river in the center of Olsztyn display less movement than the building selected for analysis selected. There is a pronounced difference in total displacement magnitude between the northern and the southern side. The majority of PS on the Northern side of the building show subsidence over 2 mm, while the PS on the Southern side move at a more varying rate, with a total subsidence of up to 0.96 mm in the center of the building. The displacement of two individual PS

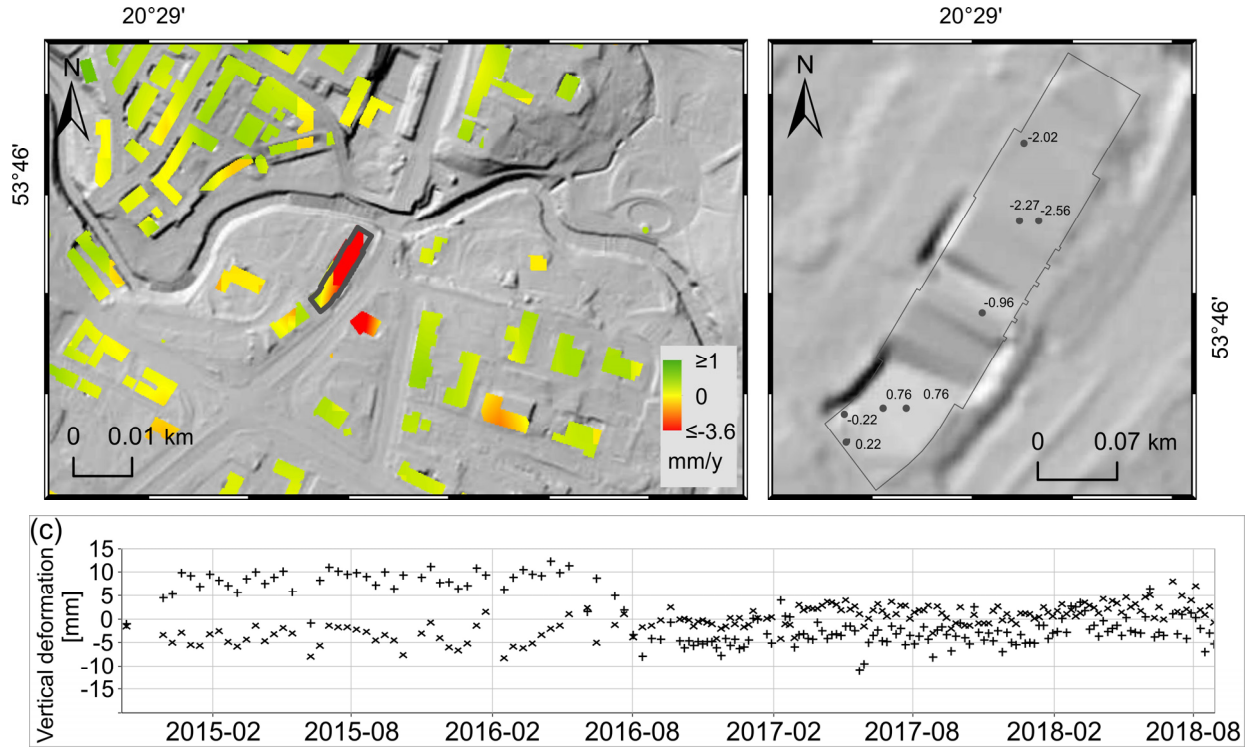

Fig. 9 The building in the city center (a) shows a map average vertical deformation rates for buildings along the river bank. The color represents the average annual vertical deformation rates from 12 October, 2014 to 31 August, 2018. The time series of two individual PS points are shown in (c) with their locations indicated in (b). Figure (b) shows location of PS measurements on the building. An outline of the building location is shown in black.

points is shown in Figure 9 (c). At the time series, it can be seen that the largest changes in the building surface occurred until April 2015, ranging from -15 to 10 mm/yr. Currently, the settlement of the building with maximum vertical deformation rate of -2.2 mm/yr can be observed.

The model was developed as a set of interpolated average Vertical values in PS target from two data sets (A29-D124, A102-D51). In the first instance the density of the PS was examined on a dataset-wide approach for each of the two data pairs. Spatial density distribution was obtained and high and low density areas were assessed. Then interpolation parameters were determined and the Kriging method (Raucoules et al., 2009) was selected. The sets were combined and a calculation was made on the basis of the semi-variogram, 20 meter search neighborhood has been used.

The model shown in Figure 10 as a map using the merge PS results shows the distribution of ground deformation from -2.9 to 2.8 mm/yr. There are positive and negative movements in the Olsztyn area (Fig. 10). The largest negative movements can be seen in the south below -1.5 mm/yr. However, in the building area, most average vertical motion rates range from -0.5 to 0.5 mm/yr.

DISCUSSION AND CONCLUSION

In this paper, the deformation in the urban area in Olsztyn is examined, with SAR data provided by the Sentinel-1 constellation. Some of the most important aspects related to Sentinel-1 SAR interferometry are also described. Calculations for Olsztyn for the first time were based on Copernicus Sentinel-1 mission data. The study of deformation area is presented using Multi-Temporal InSAR methods for small ground movement monitoring. The PSInSAR algorithm implementation used in the Stanford Method for Persistent Scatterers (StaMPS) method was chosen here. The related times series analysis makes it possible to determine the spatial and temporal variability of terrain. 644 interferograms were calculated, from which an average deformation in range from -4 to 3.3 mm/yr in the LOS direction over an area of ~ 580 km^2 was obtained. The vertical urban deformation measurements in the Olsztyn area allowed to identify the subsidence areas. The displacement patterns show that, there is little ground movement across Olsztyn, but many noticeable areas of significant movement can be distinguished, both up and down (Fig. 5). Systematic monitoring of urban infrastructure, especially communication or technical infrastructure, can be used to plan maintenance

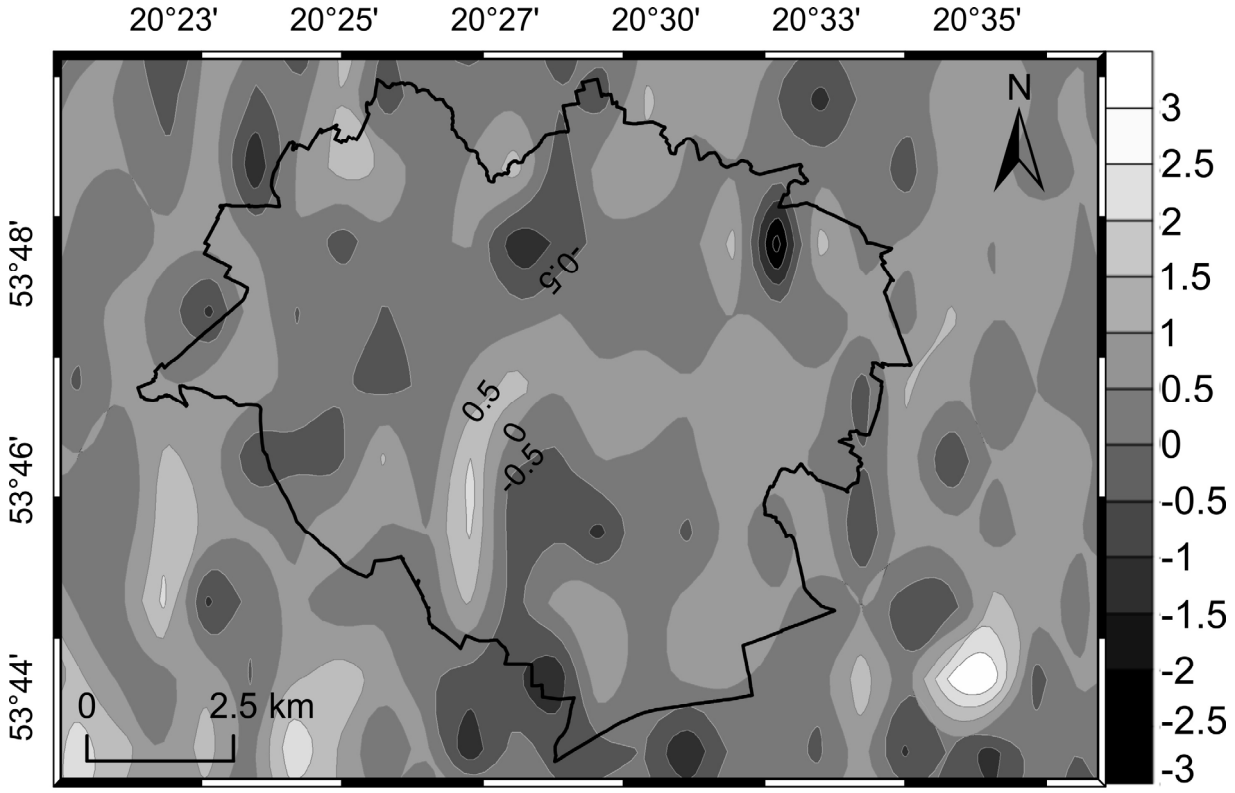

Fig. 10 The average vertical deformation measurements calculated for the period from October 2014 to August 2018, it is presented as a contour map, for the administrative border of Olsztyn (black line).

activities as well as to assess the risk associated with this infrastructure.

PS data should have been compared with measurements obtained by other geodetic measurement methods. Also the measured PS points with need to be complete with more accurate corner reflector signals data. Continuous observation will allow to understand current and future deformation changes occurring in the studied area.

The PSI method becomes an indispensable tool for monitoring the surface motion in urban environments (Wang et al., 2019). Interferometric SAR can detect surface movements with an accuracy of a few millimeters per year and can provide an accurate tool for monitoring of land subsidence, structural damage and underground construction to improve safety and reduce economic loss (ESA Standard Document, 2013). Research that was conducted in various urban areas: Berlin, Leipzig (Haghighi and Motagh, 2017), Rome (Delgado Blasco et al., 2019), London (Bischoff et al., 2019), Paris (Koudogbo et al., 2019) and Los Angeles (Khorrami et al., 2019) have demonstrated the capability and great potential of Sentinel-1A/B (S-1) TOPS, TerraSAR-X and method PSI for monitoring slow deformation, including ground, single buildings and infrastructures. Using the StaMPS algorithm in Berlin, Haghighi and Motagh (2017), determined that from during October 2014 to January 2017 the deformation in the south-eastern part of Berlin was from -4 to 1 mm/yr. In work by Bischoff et al. (2019) total displacement in the Line of Sight was determined. It was from -20 to 20 mm/yr, of 1 788 295 Permanent Scatterers (PS) and Distributed Scatterers (DS) based on 150 TerraSAR-X scenes acquired between 01 May, 2011 and 28 April, 2017. In paper by Blasco et al. (2018) obtained information on average LOS deformation rate was from -10 to 2 mm/yr over Rome and its surroundings using 160 Sentinel-1A images over the period March 2015 to April 2018. Khorrami et al. (2019) in their work used 29 Sentinel-1A acquisitions from June 2017 to May 2018 to estimate the deformation rate in Los Angeles between -30 to 10 mm/yr.

Vertical movements of the earth's crust occurring in Poland have been studied mainly based on leveling data, which in some works was analyzed together with data from mareograph so far. On the maps of speed of vertical movements for the area of Poland from 1985 (Wyrzykowski, 1987) and from 2006 (Kowalczyk, 2005) determined on the basis of leveling data in relation to the average sea level, a characteristic subsidence of the Olsztyn area can be observed. The results obtained in 1985 determine the subsidence of the terrain with an average speed of about -2 mm/yr to -2.5 mm/yr, while the results from 2006 give the size of subsidence within -2.5 mm/yr to -3 mm/yr.

To determine the value of deformation in Olsztyn, Copernicus Sentinel-1 mission data from 12 October, 2014 to 31 August, 2018 year was used. The calculated and determined average Vertical (up/down) values of the terrain deformation speed

determined for Olsztyn based on SAR data are from -2.9 to 2.8 mm/yr. The vertical motion was developed and presented as a map (Fig. 10). It can therefore be concluded that the terrain deformation rates estimated on the basis of the InSAR technique implemented in StaMPS method differ with respect to the results presented in previous studies. It is difficult to compare the deformation velocities between the studies, due to the different datasets employed and analyzed periods. It must be remembered that InSAR methods determine relative displacement, not absolute movement.

The results, which were presented in the paper, show the possibilities of using InSAR data in monitoring urban infrastructure. The Sentinel data set has significant advantages over other monitoring techniques, especially the density of measuring points over a large area, measurement accuracy of several mm and an average two-day measurement frequency for each point over several years, creating great opportunities for studying measuring deformation. There is a growing interest in a wide range of topics in which InSAR satellite data can play a role. New applications and methodologies are being developed to detect areas exposed to specific processes. The challenge is to obtain results from time series to a near real-time, where current deformation data will be provided on an ongoing basis.

ACKNOWLEDGMENTS

Thank you Tomasz Sidorowicz from University of Warmia and Mazury in Olsztyn (Faculty of Geodesy, Geospatial and Civil Engineering, Institute of Geodesy) for technical support.

Thank you contributors: Andy Hooper (Lead), David Bekaert, Karsten Spaans, Ekbal Hussain, Mahmut Arikan, Anneleen Oyen, Miguel Caro Cuenca, Jose Manuel Delgado Blasco other community members for provide the StaMPS and TRAIN software package freely available. The original version StaMPS was developed at Stanford University but subsequent development has taken place mainly at the University of Iceland, Delft University of Technology and the University of Leeds. In addition, there have been community contributions.

REFERENCES

Annex to the Commission implementing decision on the adoption of the Work programme 2018 and on the financing of the Copernicus Programme: 2018.

Bamler, R. and Hartl, P.: 1999, Synthetic aperture radar interferometry. Inverse Probl., 14, 4. DOI: 10.1088/0266-5611/14/4/001

Bekaert, D.P.S., Walters, R.J., Wright, T.J., Hooper, A.J. and Parker, D.J.: 2015, Statistical comparison of InSAR tropospheric correction techniques. Remote Sens. Environ., 170, 1, 40–47. DOI: 10.1016/j.rse.2015.08.035

Berardino, P., Fornaro, G., Lanari R. and Sansosti, E.: 2002, A new algorithm for surface deformation monitoring based on small baseline differential SAR interferograms. IEEE Trans. Geosci. Remote Sens., 40, 11, 2375–2383. DOI: 10.1109/TGRS.2002.803792

Bischoff, C.A., Ghail, R.C., Mason, P.J., Ferretti, A. and Davis, J.A.: 2019, Photographic feature: Revealing mm-scale ground movement in London using SqueeSAR™. Q. J. Eng. Geol. Hydroge. DOI: 10.1144/qjegh2018-075

Budillon, A., Crosetto, M., Monserrat, O., Johnsy, A.C., Krishnakumar, V. and Schirinzi, G.: 2018, Comparison of persistent scatterer interferometry and SAR tomography using Sentinel-1 in urban environment. Remote Sens., 10, 12. 1306. DOI: 10.3390/rs10121986

Delgado Blasco, J.M., Foumelis, M., Stewart, Ch. and Hooper, A.: 2019, Measuring urban subsidence in the Rome metropolitan area (Italy) with Sentinel-1 SNAP-StaMPS persistent scatterer interferometry. Remote, Sens., 11, 2, 129. DOI: 10.3390/rs11020129

ESA Standard Document: Sentinel-1 User Handbook: 2013.

Ferretti, A.: 2014, Satellite InSAR data; Reservoir Monitoring from Space (EET 9). EAGE Publications, 166 pp.

Ferretti, A., Colombo, D., Fumagalli, A., Novali, F. and Rucci, A.: 2015, InSAR data for monitoring land subsidence: time to think big. Proceedings of the International Association of Hydrological Sciences, 372, 331–334. DOI: 10.5194/piahs-372-331-2015

Ferretti, A., Fumagalli, A., Novali, F., Prati, C., Rocca, F. and Rucci, A.: 2011, A new algorithm for processing interferometric data-stacks: SqueeSAR. IEEE Trans. Geosci. Remote Sens., 49, 9, 3460–3470. DOI: 10.1109/TGRS.2011.2124465

Ferretti, A., Prati, C. and Rocca, F.: 1999, Permanent Scatterers in SAR Interferometry. IEEE 1999 International Geoscience and Remote Sensing Symposium. IGARSS'99, 3, 1528-1530. DOI: 10.1109/IGARSS.1999.772008

Ferretti, A., Prati, C. and Rocca, F.: 2001, Permanent scatterers in SAR interferometry. IEEE Trans. Geosci. Remote Sens., 39, 1, 8–20. DOI: 10.1109/36.898661

Ferretti, A., Savio G., Barzaghi, R., Borghi, A., Musazzi, S., Novali, F., Prati, C. and Rocca, F.: 2007, Submillimeter accuracy of InSAR time series: Experimental validation. IEEE Trans. Geosci. Remote Sens., 45, 5, 1142–1153. DOI: 10.1109/TGRS.2007.894440

Foumelis, M.: 2018, Vector-based approach for combining ascending and descending persistent scatterers interferometric point measurements. Geocarto Int., 33, 1, 38–52. DOI: 10.1080/10106049.2016.1222636

Goldstein, R.: 1995, Atmospheric limitations to repeat-pass interferometry. Geophys. Res. Lett., 22, 18, 2517–2520. DOI: 10.1029/95GL02475

Haghighi, M.H. and Motagh, M.: 2017, Sentinel-1 InSAR over Germany: Large-scale interferometry, atmospheric effects and ground deformation mapping. Zeitschrift fuer Geodasie, Geoinformation und Landmanagement, 142, 4, 245–256. DOI: 10.12902/zfv-0174-2017

Hanssen, R.F.: 2001, Radar interferometry: Data interpretation and error analysis, 2, XVIII, 308. DOI: 10.1007/0-306-47633-9

Hooper, A., Segall, P. and Zebker, H.A.: 2007a, Persistent scatterer InSAR for crustal deformation analysis, with application to Volcán Alcedo, Galápagos. J. Geophys. Res., 112. DOI: 10.1029/2006JB004763

Hooper, A. and Zebker, H.A.: 2007b, Phase unwrapping in three dimensions with application to InSAR time series. J. Opt. Soc. Am. A, 24, 9, 2737–2747. DOI: 10.1364/josaa.24.002737

Hooper, A., Zebker, H., Segall, P. and Kampes, B.: 2004, A new method for measuring deformation on volcanoes and other natural terrains using InSAR persistent scatterers. Geophys. Res. Lett., 31, 23, L23611. DOI: 10.1029/2004GL021737

Hu, J., Li, Z.W., Ding, X.L., Zhu, J.J., Zhang, L. and Sun, K.: 2014, Resolving three-dimensional surface displacements from InSAR measurements: A review. Earth-Sci. Rev., 133, 1–17. DOI: 10.1016/j.earscirev.2014.02.005

Khorrami, M., Alizadeh, B., Ghasemi Tousi, E., Shakerian, M., Maghsoudi, Y. and Rahgozar, P.: 2019, How groundwater level fluctuations and geotechnical properties lead to asymmetric subsidence: A PSInSAR analysis of land deformation over a transit corridor in the Los Angeles metropolitan area. Remote Sens., 11, 4, 377. DOI: 10.3390/rs11040377

Koudogbo, F., Urdiroz, A., Garcia Robles, J., Chapron, G., Lebon, G., Fluteaux, V. and Priol, G: 2019, Radar interferometry as an innovative solution for monitoring the construction of the Grand Paris Express metro network – First results. 4 th Joint International Symposium on Deformation Monitoring. Proceedings of the World Tunnel Congress 2018

Kowalczyk, K.: 2005, Determination of land uplift in the area of Poland. 6th International Conference Environment Engineering, vol. 2, 903-907.

Krishnakumar, V., Monserrat, O., Crosetto, M. and Crippa, B.: 2018, Atmospheric phase delay in Sentinel SAR interferometry. Int. Arch. Photogramm. Remote Sens. Spat. Inf. Sci., XLII-3, 741–744. DOI: 10.5194/isprs-archives-XLII-3-741-2018

Monti-Guarnieri, A., Parizzi, F., Pasquali, P., Prati, C., Rocca, F.: 1993, SAR interferometry experiments with ERS-1, IEEE International Geoscience and Remote Sensing Symposium, 3, 991-993. DOI: 10.1109/IGARSS.1993.322168

Nowicki, Z.: 2007, Guidebook of the Polish State Hydrogeological Survey, Polish Geological Institute.

Osmanoğlu, B., Sunar, F., Wdowinski, S. and Cabral-Cano, E.: 2016, Time series analysis of InSAR data: Methods and trends. ISPRS J. Photogramm. Remote Sens., 115, 90–102. DOI: 10.1016/j.isprsjprs.2015.10.003

Perski, Z. and Wojciechowski, T.: 2017, Monitoring of land surface subsidence in 3 selected gas exploration locations in land formations. Task report 3.2., Review of interferometric analysis methods to choose the optimal InSAR measurement method.

Raucoules, D., Bourgine, B., de Michele, M, Le Cozannet, G., Closset, L., Bremmer, Ch., Veldkamp, H., Tragheim, D., Bateson, L., Crosetto, M., Agudo M., Engdal, M.: 2009, Validation and intercomparison of Persistent Scatterers interferometry: PSIC4 project results. J. Appl. Geophys., 68, 3, 335–347. DOI: 10.1016/j.jappgeo.2009.02.003

Rosen, P.A., Hensley, S., Zebker, H.A., Webb, F.H. and Fielding, E.J.: 1996, Surface deformation and coherence measurements of Kilauea Volcano, Hawaii, from SIR-C radar interferometry, 101, E10, 23109–23125. DOI: 10.1029/96JE01459

Samiei-Esfahany, S., Hanssen, R., Thienen-Visser, K. and Muntendam-Bos, A.G.: 2009, On the effect of horizontal deformation on InSAR subsidence estimates. Fringe 2009 Workshop, Frascati, Proceedings.

Tre Altamira: 2010, Interferometric Synthetic Aperture RADAR. An Introduction for Users of InSAR Data. Conference Proceedings.

Vollrath, A., Zucca, F., Bekaert, D., Bonforte, A., Guglielmino, F., Hooper, A. and Stramondo, S.: 2017, Decomposing DInSAR time-series into 3-D in combination with GPS in the case of low strain rates: An application to the Hyblean Plateau, Sicily, Italy. Remote Sens., 9, 1, 26. DOI: 10.3390/rs9010033

Wang, Z., Balz, T., Zhang, L., Perissin, D. and Liao, M.: 2019, Using TSX/TDX pursuit monostatic SAR stacks for PS-InSAR analysis in urban areas. Remote Sens., 11, 26. DOI: 10.3390/rs11010026

Wortham, C.B.: 2014, Vector deformation time-series from spaceborne motion compensation InSAR processors. Dissertation.

Wyrzykowski, T.: 1987, A new determination of velocity of recent vertical movements of the Earth crust on the territory of Poland. Prace IGIK, 34, 1, 78, (in Polish).

Yagüe-Martínez, N., Prats-Iraola, P., González, F.R., Brcic, R., Shau, R., Geudtner, D., Eineder, M. and Bamler, R.: 2016, Interferometric processing of Sentinel-1 TOPS data. IEEE Trans. Geosci. Remote Sens., 54, 4, 2220–2234. DOI: 10.1109/tgrs.2015.2497902

Zebker, H.A. and Goldstein, R.M.: 1986, Topographic mapping from interferometric synthetic aperture radar observations. J. Geophys. Res., 91, B5, 4993–4999. DOI: 10.1029/JB091iB05p04993

Zebker, H.A. and Villasenor, J.: 1992, Decorrelation in interferometric radar echoes. IEEE Trans. Geosci. Remote Sens., 30, 5, 950–959. DOI: 10.1109/36.175330